applied optics

Computational structured illumination

HIROAKI MATSUI, RYOICHI HORISAKI,* AND JUN TANIDA

Department of Information and Physical Sciences, Graduate School of Information Science and Technology, Osaka University, 1-5 Yamadaoka, Suita, Osaka 565-0871, Japan
**Corresponding author: r.horisaki@ist.osaka-u.ac.jp*

Received 31 July 2015; revised 14 September 2015; accepted 15 September 2015; posted 15 September 2015 (Doc. ID 247164); published 8 October 2015

We propose a computational structured illumination method for flexible object observation and measurement, which is a gradual extension of computational imaging. In the method, the impulse responses of illumination (IRIs) are observed in advance, and then the optical reflection for an arbitrary illumination pattern is generated by the superposition of the impulse responses. As a benefit of the method, illumination patterns can be easily designed and adjusted for different purposes without physical experiments after the IRI observation, and the desired information can be reconstructed with the same process as that used in conventional-structure illumination methods. A high-precision optical setup does not have to be maintained physically because it is virtualized in a computer. We experimentally demonstrated three-dimensional shape measurement and signal separation between direct- and internal-reflection components using the proposed method.

OCIS codes: (110.1758) Computational imaging; (110.2945) Illumination design; (150.6910) Three-dimensional sensing; (290.4210) Multiple scattering.

http://dx.doi.org/10.1364/AO.54.008742

1. INTRODUCTION

Structured illumination (SI) is an effective technique for observing objects with a variety of modalities. In SI, an object is illuminated with specially designed patterns, and then the target information, which is veiled under a uniform illumination, is extracted via postprocessing in a computer. The technique has been applied to various problems in many fields, including industry and biomedicine. A typical example is a three-dimensional shape measurement with a projection of a fringe pattern or a gray code [1–6]. Direct- and internal-reflection signals can be separated using a checker pattern [7,8]. In microscopy, superresolution has been achieved with fringe pattern projection to fold high-spatial-frequency components into the effective aperture [9,10].

In these methods, the observed signals are processed to reconstruct the target information, which is a promising framework known as computational imaging. In spite of the flexibility of computational processes, optical processes must be carefully prepared to achieve effective imaging. For SI, the illumination patterns are designed for given problems and are adjusted for individual objects [11]. This adjustment process is a bottleneck in SI systems because it is mainly executed manually and requires several trials with projections of different patterns. The need to prepare illumination patterns restricts the flexibility and throughput of SI.

As is well-known, image-based rendering is a popular technique in computer graphics [12–14]. Arbitrary images can be generated for any camera and under any illumination conditions. For the case of image-based illumination, the impulse responses of illumination (IRIs) are observed in advance [15]. IRIs are images with pinpoint illumination at a unit area on the object surface. Because any illumination can be expressed as a suitable superposition of IRIs, it can be linearly calculated from the IRIs. This technique has been applied to face rendering under arbitrary illumination [15], texture recognition [16], computational displays reflecting ambient illumination with free viewpoints [17], and so on.

In this paper, we describe the concept of computational structured illumination, in which an object's illumination is integrated within the framework of computational imaging. The IRIs of the object are captured in advance, and then the optical reflection for any illumination pattern is generated. The signals are processed to retrieve the target information with the same process as that used in conventional SI. One benefit of this method is that we can design illumination patterns for different purposes and can easily adjust them for individual objects without trials in the analog process. In addition, a high-precision optical setup does not have to be physically maintained after the IRI observation because it is virtualized in a computer in this case.

2. PROPOSED SCHEME

Figure 1 shows the differences between conventional SI and computational SI. As shown in Fig. 1(a), a structured pattern

is used for illumination. The captured image is processed using an appropriate calculation, such as a Fourier fringe analysis and a max–min analysis, for the target application to reconstruct the target information.

The computational SI method is composed of three steps, which are shown in Fig. 1(b). Step 1, which we refer to as an analog process, is the acquisition of the IRIs. Step 2 is a computational synthesis of optical reflections for a designed illumination pattern using a matrix-based calculation with the IRIs. Step 3 is postprocessing according to an SI method to reconstruct the output. Steps 2 and 3 are implemented by digital processing.

A set of IRIs is expressed as a matrix, which is denoted as $\boldsymbol{A} \in \mathbb{R}^{N_{\text{cam}} \times N_{\text{proj}}}$. Here, N_{proj} is the total number of pixels in a projector for illuminating an object with the inputs (impulses), and N_{cam} is the total number of pixels in a camera for capturing the outputs (responses) from the object. The elements of an IRI are arranged in each column of the IRI matrix $\boldsymbol{A}$, where the horizontal and vertical coordinates correspond to the irradiant and radiant positions, respectively, as shown in Fig. 2. Once the IRI matrix $\boldsymbol{A}$ is observed, a camera image $\boldsymbol{y} \in \mathbb{R}^{N_{\text{cam}} \times 1}$ for the case where an arbitrary illumination pattern $\boldsymbol{x} \in \mathbb{R}^{N_{\text{proj}} \times 1}$ is projected onto the object is calculated as

$$\boldsymbol{y} = \boldsymbol{A}\boldsymbol{x}. \tag{1}$$

Both the camera image $\boldsymbol{y}$ and the illumination pattern $\boldsymbol{x}$ are column vectors. Step 2 of the proposed method corresponds to Eq. (1) and Fig. 2.

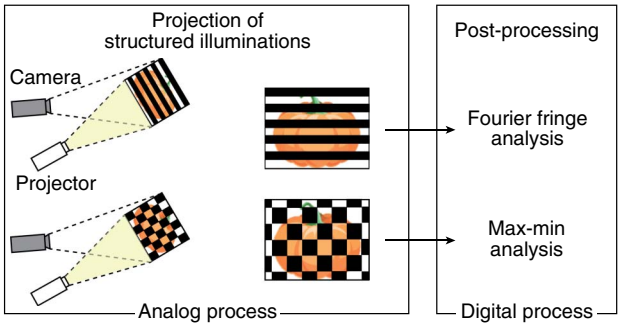

(a)

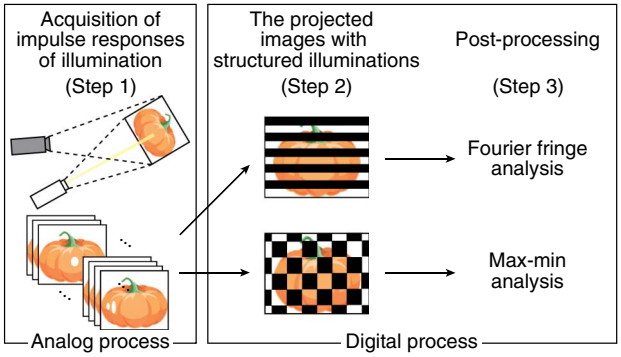

(b)

Fig. 1. Schematic diagrams of (a) a conventional-structure illumination-based system and (b) a computational structured illumination-based system.

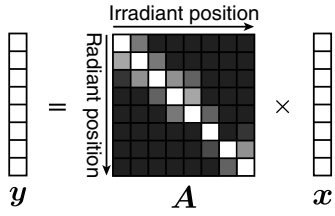

Fig. 2. Computational synthesis of structured illumination.

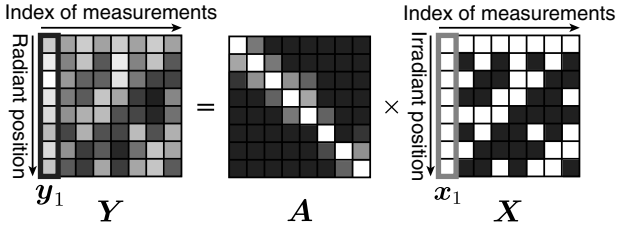

Fig. 3. Relationship between the input and output datasets.

The IRI matrix $\boldsymbol{A}$ can be calculated using the datasets of the input vector $\boldsymbol{x}$ and the output vector $\boldsymbol{y}$ in Eq. (1) [18]. The input and output datasets are described as matrices $\boldsymbol{X} \in \mathbb{R}^{N_{\text{proj}} \times M}$ and $\boldsymbol{Y} \in \mathbb{R}^{N_{\text{cam}} \times M}$, where the columns of the input and output matrices are the input and output vectors, respectively, as shown in Fig. 3. The horizontal coordinates of the matrices $\boldsymbol{X}$ and $\boldsymbol{Y}$ correspond to the index of the measurements of vectors $\boldsymbol{x}$ and $\boldsymbol{y}$. M is the number of measurements. Their relationship is written as

$$\boldsymbol{Y} = \boldsymbol{A}\boldsymbol{X}. \tag{2}$$

This means that the IRI matrix $\boldsymbol{A}$ is estimated from the input and output matrices $\boldsymbol{X}$ and $\boldsymbol{Y}$ by taking the inverse of Eq. (2) as follows:

$$\hat{\boldsymbol{A}} = \boldsymbol{Y}\boldsymbol{X}^{-1}. \tag{3}$$

The input matrix $\boldsymbol{X}$ is arbitrarily chosen. In this paper, we chose the Hadamard matrix for $\boldsymbol{X}$ to improve the signal-to-noise ratio of the recovered IRI matrix $\hat{\boldsymbol{A}}$ [18]. The Hadamard matrix is known to be the optimal matrix $\boldsymbol{X}$ for observing the IRI matrix $\boldsymbol{A}$ without any prior information on the IRI matrix, supposing that there is white additive noise on the measurements. The signal-to-noise ratio of IRI matrix acquisition based on the Hadmard matrix is $\sqrt{M}/2$ times higher than that of IRI matrix acquisition based on the identity matrix, where the IRI matrix is captured by point scanning [19]. The number of measurements can be significantly reduced based on compressive sensing (CS) [20–23]. Step 1 of the proposed method in Fig. 1(b) corresponds to Eq. (2) and Fig. 3.

3. EXPERIMENTAL DEMONSTRATIONS

To verify the effectiveness of our scheme, we experimentally compared the results of three-dimensional shape measurement and signal separation for direct- and internal-reflection signals in conventional and computational SI. The experimental setup

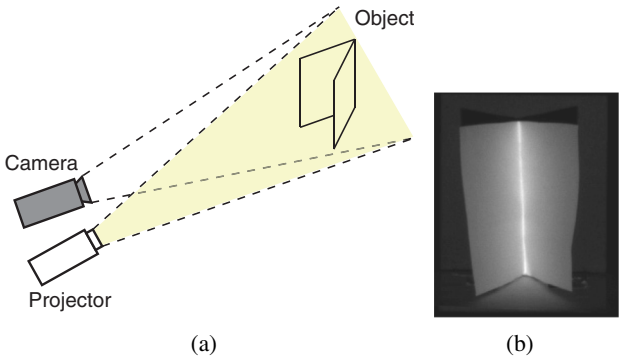

Fig. 4. Experimental setup. (a) The optical setup. (b) The object under uniform illumination.

was composed of a monochrome CCD camera (PL-B953U manufactured by PIXELINK; 1024 pixels × 768 pixels with a pitch of 4.65 μm × 4.65 μm), a projector (EB1910 manufactured by EPSON; 1024 × 768 pixels), and an object, as shown in Fig. 4(a). The object was a valley-folded sheet of white paper, as shown in Fig. 4(b), and the distance between the object and both the camera and the projector was 81 cm.

We observed the IRI matrix $\boldsymbol{A}$ based on the Hadamard illumination described in the previous section. In the experiment, N_{cam} was 40001 (221 × 181 pixels), N_{proj} was 1254 (38 × 33 pixels), and M was 1254. The reconstructed IRI matrix $\hat{\boldsymbol{A}}$ is shown in Fig. 5. Generally, IRI matrices are known to be very sparse and compressible, as indicated in this figure, where the ratio of the number of nonzero coefficients to the number of total elements in the IRI matrix was about 0.1%. As a result, the number of measurements can be reduced based on the sparsity [22].

A. Three-Dimensional Shape Measurement

The first demonstration was the three-dimensional shape measurement with Fourier transform profilometry. First, we performed the original method as a reference. The captured image of the object, onto which a fringe pattern was projected, is shown in Fig. 6(a). The pitch and angle of the fringe pattern

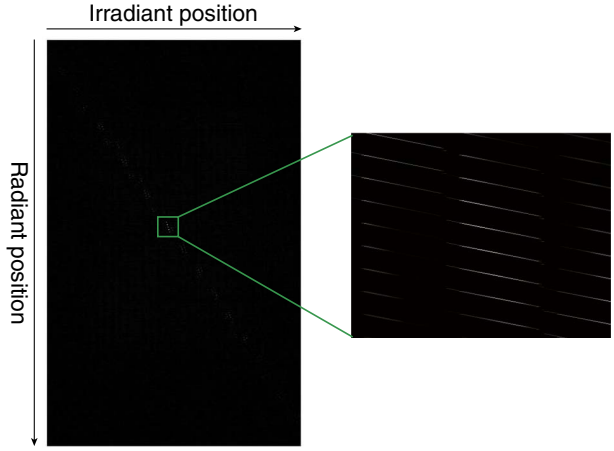

Fig. 5. Reconstructed matrix of the impulse responses of illumination.

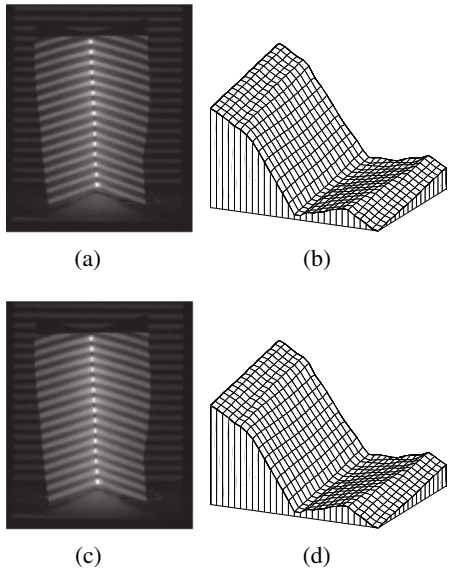

Fig. 6. Experimental data in the three-dimensional shape measurement. (a) The captured image and (b) the shape map using the conventional method. (c) The computationally captured image and (d) the shape map using our proposed method.

were experimentally chosen. The phase of the distorted fringe was calculated by using the Fourier transform [1]. Then, the phase was unwrapped [24]. The reconstruction result is shown in Fig. 6(b), which shows that the valley-folded shape of the object was obtained.

Figure 6(c) shows the computationally synthesized image based on our proposed method with the same pattern as in the reference method. It was calculated with the IRI matrix in Fig. 5 and Eq. (1). A shape map with the same reconstruction procedure as that used in the reference method is shown in Fig. 6(d). The images obtained with the fringe pattern projection and the shape map agreed with each other. The peak signal-to-noise ratio (PSNR) between Figs. 6(a) and 6(c) was 36.9 dB, and the PSNR between Figs. 6(b) and 6(d) was 48.2 dB.

B. Separation between Direct- and Internal-Reflection Components in a Scene

The second demonstration was signal separation between direct- and internal-reflection components with a checker pattern [7]. First, we performed the original method as a reference. The checker pattern was shifted 5 times in both the horizontal and vertical directions with an interval of 3/4 of the checker size. The total number of captured images was 25. The parameters of the checker pattern and its shift were chosen experimentally. One of the captured images is shown in Fig. 7(a). The maximum and minimum intensities at each spatial point were obtained, and then the direct- and internal-reflection components were extracted. The separation results are shown in Figs. 7(b) and 7(c). The direct-reflection component in Fig. 7(b) shows a strong intensity around the bottom of the valley because this part directly faces the projector and the camera. The bright areas in the internal-reflection component in Fig. 7(c) are the sides of the valley, where multiple reflections occurred.

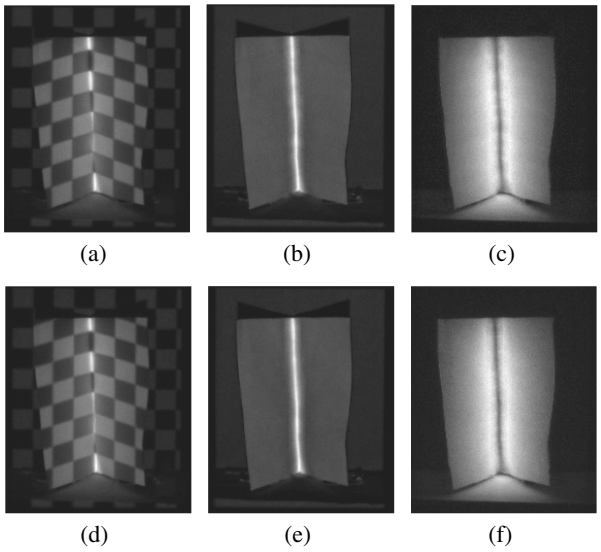

Fig. 7. Experimental data for separation of direct- and internal-reflection components in a scene. (a) One of the 25 captured images, and the (b) direct- and (c) internal-reflection components using the conventional method. (d) One of the 25 computationally captured images, and the (e) direct- and (f) internal-reflection components using our proposed method.

The captured images were computationally synthesized with the IRI matrix in Fig. 5 and Eq. (1) using our proposed method, as shown in Fig. 7(d). Figures 7(e) and 7(f) are the separated signals from the images synthesized using the same procedure as the reference. They are in good agreement with those of the conventional SI method in Figs. 7(a)–7(c). The average of the PSNRs of the 25 captured images obtained with the reference method and our scheme was 39.0 dB. The PSNRs of the direct- and internal-reflection components with the reference method and our scheme were 37.0 and 26.1 dB, respectively.

4. CONCLUSIONS

We have proposed a computational SI scheme in which arbitrary illumination patterns are computationally generated as an extension of computational imaging. In our method, the optical reflections for any illumination patterns are synthesized from IRIs acquired in advance. Then, the object's information is extracted from the synthesized images according to the conventional SI method. This method has the advantage that suitable illumination patterns can be designed for various SI techniques and can be adjusted for individual objects without analog trials. A high-precision optical setup does not have to be physically maintained after the IRI observations. Our approach to the virtualization of imaging systems can be extended not only to illumination, but also to image acquisition [25].

We experimentally verified our method by conducting two demonstrations. The first demonstration was a three-dimensional shape measurement, and the second was a signal separation between the direct- and internal-reflection components in a scene. The experimental results verified the effectiveness of the proposed method. Although the object in the demonstrations was simple, in order to clarify the concept of computational SI, which is a virtualization of illumination, our method can be applied to more complicated objects by employing a high-resolution camera and projector, and by suitable postprocessing.

An important issue with our method is the acquisition cost of the IRI matrix. Compressive sensing (CS) [20] provides an effective solution to this problem. CS is a powerful framework for reducing the number of sampling steps by exploiting the sparsity of objects. The IRI matrix was very sparse and compressible, as shown in Fig. 5. CS-based methods for IRI matrix acquisition can be applied to our method [22,23]. Such a CS-based approach reduces the cost of observation and enhances the advantages of computational SI.

REFERENCES

1. M. Takeda, H. Ina, and S. Kobayashi, "Fourier-transform method of fringe-pattern analysis for computer-based topography and interferometry," J. Opt. Soc. Am. **72**, 156–160 (1982).
2. D. Scharstein and R. Szeliski, "High-accuracy stereo depth maps using structured light," in *Proceedings of IEEE Conference on Computer Vision and Pattern Recognition* (IEEE, 2003), pp. 195–202.
3. J. Geng, "Structured-light 3D surface imaging: a tutorial," Adv. Opt. Photon. **3**, 128–160 (2011).
4. C. Je, S. Lee, and R.-H. Park, "High-contrast color-stripe pattern for rapid structured-light range imaging," in *Computer Vision—ECCV* **3021** of Lecture Notes in Computer Science (Springer, 2004), pp. 95–107.
5. C. Je, S. W. Lee, and R. H. Park, "Colour-stripe permutation pattern for rapid structured-light range imaging," Opt. Commun. **285**, 2320–2331 (2012).
6. R. Zou, Y. Zhou, Y. Yu, and S. Du, "A novel locally adaptive dynamic programming approach for color structured light system," in *Advances in Visual Computing*, Vol. **7431** of Lecture Notes in Computer Science (Springer, 2012), pp. 372–381.
7. S. K. Nayar, G. Krishnan, M. D. Grossberg, and R. Raskar, "Fast separation of direct and global components of a scene using high frequency illumination," ACM Trans. Graph. **25**, 935–944 (2006).
8. T. Ando, R. Horisaki, T. Nakamura, and J. Tanida, "Single-shot acquisition of optical direct and global components using single coded pattern projection," Jpn. J. Appl. Phys. **54**, 042501 (2015).
9. M. G. Gustafsson, "Surpassing the lateral resolution limit by a factor of two using structured illumination microscopy," J. Microsc. **198**, 82–87 (2000).
10. P. Kner, B. B. Chhun, E. R. Griffis, L. Winoto, and M. G. L. Gustafsson, "Super-resolution video microscopy of live cells by structured illumination," Nat. Methods **6**, 339–342 (2009).
11. B. Zhao and A. Asundi, "Discussion on spatial resolution and sensitivity of Fourier transform fringe detection," Opt. Eng. **39**, 2715–2719 (2000).
12. L. McMillan and G. Bishop, "Plenoptic modeling: an image-based rendering system," in *Proceedings of ACM SIGGRAPH* (SIGGRAPH, 1995), pp. 39–46.
13. M. Levoy and P. Hanrahan, "Light field rendering," in *Proceedings of ACM SIGGRAPH* (SIGGRAPH, 1996), pp. 31–42.
14. H. Shum and S. B. Kang, "A review of image-based rendering techniques," Proc. SPIE **4067**, 2–13 (2000).
15. P. Debevec, T. Hawkins, C. Tchou, H. Duiker, W. Sarokin, and M. Sagar, "Acquiring the reflectance field of a human face," in *Proceedings of ACM SIGGRAPH* (SIGGRAPH, 2000), pp. 145–156.
16. K. J. Dana, B. van Ginneken, S. K. Nayar, and J. J. Koenderink, "Reflectance and texture of real-world surfaces," ACM Trans. Graph. **18**, 1–34 (1999).
17. R. Horisaki and J. Tanida, "Reflectance field display," Opt. Express **21**, 11181–11186 (2013).

18. Y. Y. Schechner, S. K. Nayar, and P. N. Belhumeur, "A theory of multiplexed illumination," in *Proceedings of IEEE International Conference on Computer Vision* (IEEE, 2003), pp. 808–815.
19. N. Ratner, Y. Y. Schechner, and F. Goldberg, "Optimal multiplexed sensing: bounds, conditions and a graph theory link," Opt. Express **15**, 17072–17092 (2007).
20. D. L. Donoho, "Compressed sensing," IEEE Trans. Inf. Theory **52**, 1289–1306 (2006).
21. E. J. Candes and M. B. Wakin, "An introduction to compressive sampling," IEEE Signal Process. Mag. **25**(2), 21–30 (2008).
22. P. Peers, D. K. Mahajan, B. Lamond, A. Ghosh, W. Matusik, R. Ramamoorthi, and P. Debevec, "Compressive light transport sensing," ACM Trans. Graph. **28**, 1–18 (2009).
23. Y. Tampa, R. Horisaki, and J. Tanida, "Experimental verification of compressive reflectance field acquisition," Appl. Opt. **53**, 3157–3163 (2014).
24. T. R. Judge and P. J. Bryanston-Cross, "A review of phase unwrapping techniques in fringe analysis," Opt. Lasers Eng. **21**, 199–239 (1994).
25. T. Nakamura, R. Horisaki, and J. Tanida, "Computational phase modulation in light field imaging," Opt. Express **21**, 29523–29543 (2013).